

Direct Detection of Ultralight Dark Matter via Charged Lepton Flavor Violation

Innes Bigaran,^{1,2} Patrick J. Fox,² Yann Gouttenoire,^{3,4}
 Roni Harnik,² Gordan Krnjaic,^{2,5,6} Tony Menzo,⁷ and Jure Zupan⁷

¹*Department of Physics & Astronomy, Northwestern University, 2145 Sheridan Road, Evanston, IL 60208, USA*

²*Theory Division, Fermilab, P.O. Box 500, Batavia, IL 60510, USA*

³*School of Physics and Astronomy, Tel-Aviv University, Tel-Aviv 69978, Israel*

⁴*PRISMA Cluster of Excellence & Mainz Institute for Theoretical Physics,
 Johannes Gutenberg University, Staudingerweg 7, 55099 Mainz, Germany*

⁵*Department of Astronomy and Astrophysics, University of Chicago, Chicago, IL 60637*

⁶*Kavli Institute for Cosmological Physics, University of Chicago, Chicago, IL 60637*

⁷*Department of Physics, University of Cincinnati, Cincinnati, Ohio 45221, USA*

(Dated: March 12, 2025)

We propose a dark matter direct-detection strategy using charged particle decays at accelerator-based experiments. If ultralight ($m_\phi \ll \text{eV}$) dark matter has a misalignment abundance, its local field oscillates in time at a frequency set by its mass. If it also couples to flavor-changing neutral currents, rare exotic decays such as $\mu \rightarrow e\phi$ and $\tau \rightarrow e(\mu)\phi$ inherit this modulation. Focusing on such charged lepton flavor-violating decays, we show that sufficient event samples can enable detection of ultralight dark matter candidates at Mu3e, Belle-II, and FCC-ee.

The existence of dark matter (DM) would provide smoking-gun evidence for physics beyond the Standard Model (SM), yet its particle nature remains unknown despite decades of dedicated experiments [1]. While these searches have traditionally focused on DM masses near the weak scale, in recent years, this global effort has broadened to cover a wide range of DM masses. Such strategies incorporate techniques from diverse disciplines, including accelerator [2], condensed matter [3, 4], and atomic/molecular/optical physics [5], and their relative advantages depend greatly on the DM mass scale.

Based on the measured dark matter mass density and the Tremaine-Gunn bound [6], any self-consistent theory of “ultralight” DM *must* be both bosonic and wavelike with a present day classical field value [7]

$$\phi_c(t) = \phi_0 \cos(m_\phi t + \delta), \quad (1)$$

where m_ϕ is the DM mass, δ is an arbitrary phase. The amplitude satisfies

$$\phi_0 = \frac{\sqrt{2\rho_\phi}}{m_\phi} \simeq 2.5 \text{ TeV} \left(\frac{10^{-15} \text{ eV}}{m_\phi} \right), \quad (2)$$

where $\rho_\phi = 0.4 \text{ GeV/cm}^3$ is the local dark matter mass density [8] and ϕ is said to be “misaligned” from its potential minimum. This unique¹ description of ultralight DM offers a powerful first-principles starting point for *any* investigation into DM candidate masses in the range $10^{-21} \text{ eV} < m_\phi < 1 \text{ eV}$. Masses below 10^{-21} eV are excluded because the DM de-Broglie wavelength exceeds the scale of dwarf galaxies [9, 10].

¹ If the functional form were to substantially deviate from Eq. (1), the energy density would not redshift like non-relativistic pressureless matter [7], which would spoil cosmological structure formation. Alternatively, if ϕ were a spin-1 field, Eq. (1) would feature a polarization vector, but the time dependence and the amplitude would not be affected.

As the field in Eq. (1) modulates in time with frequency m_ϕ , interactions between ϕ and the SM fields can inherit the characteristic periodicity

$$\tau_\phi = \frac{2\pi}{m_\phi} \simeq 4 \text{ s} \left(\frac{10^{-15} \text{ eV}}{m_\phi} \right), \quad (3)$$

which may be appreciable on experimental timescales. While there is a large literature on DM-induced time variation in fundamental constants, particle masses, and nuclear spin-precession, these strategies assume flavor blind interactions between ϕ and SM fields (see [11–13] for reviews). Ultralight DM has been studied as a catalyst for time variation in the quark and lepton mixing matrices [14–20], or in the CP phase of strong interactions [21–23]. However, to date, no study has explored its possible impact on flavor violating processes.

In this *Letter*, we introduce a novel DM search strategy based on flavor changing neutral current (FCNC) transitions induced by the presence of a misaligned field. We focus on charged lepton flavor violating (CLFV) decays, and find that certain classes of dark-visible interactions can viably induce time-modulation at levels that can be probed at existing and future experiments.

As numerical examples, we show projections for a possible reanalysis of existing Belle-II data [24, 25], as well as the estimates for future Mu3e [26–28] and FCC-ee [29–31] sensitivities – these results are presented in Fig. 1. Similar analyses could be performed at many current and future CLFV experiments, including MEG-II [32–34], Mu2e [35–39], COMET [38, 40, 41], BES-III [42, 43], Super Tau Charm Factory [44–46], and CEPC [47].

Time-dependent CLFV interactions. Arguably the simplest interaction of ϕ to the SM fermions arises from the dimension-5 Higgs interaction

$$\mathcal{L}_{\text{int}} \supset \left(\frac{\phi}{\Lambda_{ij}} \right) H \bar{L}_i \ell_j \rightarrow y_{ij} \phi \bar{\ell}_i \ell_j, \quad (4)$$

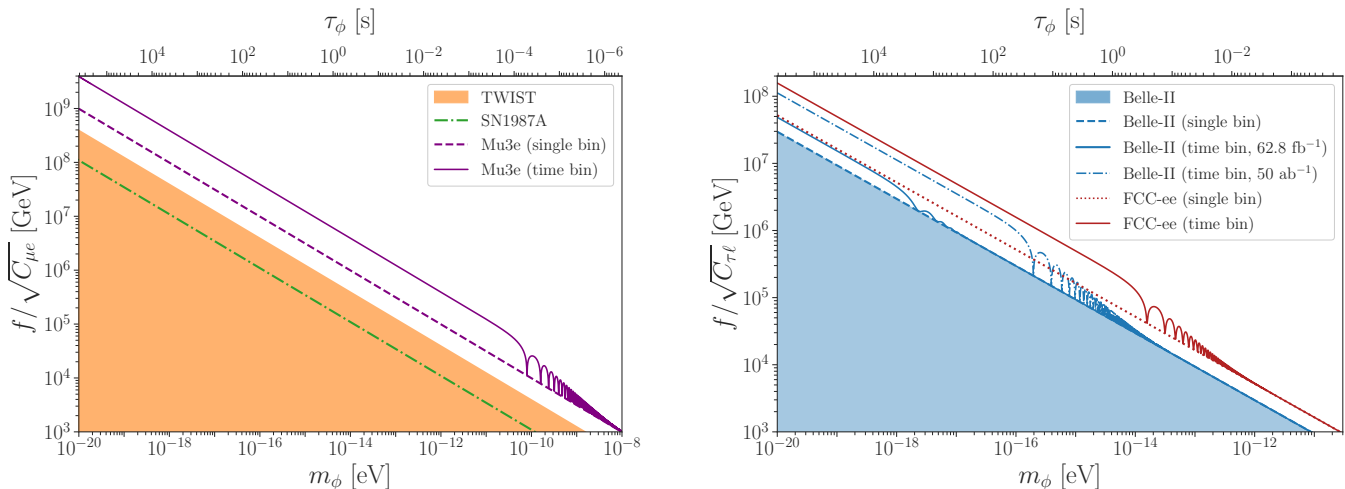


FIG. 1. Present and projected constraints on LFV couplings $f/\sqrt{C_{\mu e}}$ (left) and $f/\sqrt{C_{\tau \ell}}$ (right) for time-binned and single-bin analyses, as a function of the scalar mass, m_ϕ – see Eqs. (7) and (9). **Left:** Present constraint from TWIST [48] is shaded in yellow. The projected single-bin (dashed line) and time-binned (solid line) analysis reach from Mu3e [27, 28] are shown in purple. The astrophysical bound on $f/\sqrt{C_{\mu e}}$ from SN1987A [33, 49] is shown here as a dot-dashed green line – see main text for details. **Right:** The constraints on $f/\sqrt{C_{\tau \ell}}$ from present and projected Belle-II analyses [25] are shown here in blue: current 62.8 fb^{-1} time-integrated constraint is shaded, single-bin constraint is a dashed line and projected time-binned constraint is a solid line; the 50 ab^{-1} projected time-binned constraint is a dot-dashed line. The projected constraints from FCC-ee Tera-Z run [30] are shown in red: dotted line for single-bin analysis, and red solid line for time-binned analysis. The constraints on $C_{\tau \mu}$ and on $C_{\tau e}$ (denoted collectively here as $C_{\tau \ell}$) almost completely overlap on this logarithmic scale.

where ℓ_i is a charged fermion with flavor index i , Λ_{ij} is the cutoff scale of the interaction, $y_{ij} \equiv v/\sqrt{2}\Lambda_{ij}$ is a coupling matrix. In the last step, we set the Higgs doublet H to its vacuum expectation value $v = 246 \text{ GeV}$, and only kept the charged component of the lepton doublet L_i . The interactions in Eq. (4), however, do not lead to observable time-dependent CLFV transitions, since they face several significant challenges:

1. *Fine Tuning:* At one loop, the interactions in Eq. (4) yield large corrections to the scalar mass m_ϕ of order $\mathcal{O}(y m_\ell/4\pi)$. Generically, this is in tension with the requirement $m_\phi \ll \text{eV}$ needed to preserve the classical solution in Eq. (1). Even if ϕ couples only to the electron, the small ϕ mass condition is greatly violated unless the Yukawa couplings are exceedingly small or the ϕ potential is severely tuned.
2. *Time-independent Limits:* The off-diagonal interactions in Eq. (4) predict flavor changing processes, including the decays: $\tau \rightarrow \mu\phi$, $\tau \rightarrow e\phi$, and $\mu \rightarrow e\phi$, where the final state ϕ is invisible to experiments. For linear ϕ coupling, as in Eq. (4), these decay rates are independent of the ϕ_c background at leading order and, therefore, do not inherit time modulation. Furthermore, conventional time-averaged searches for $\ell_i \rightarrow \ell_j + \text{invisible}$ decays yield stringent limits on the cou-

plings [25, 33, 50]

$$|y_{\tau e}|, |y_{\tau \mu}| \lesssim 2 \times 10^{-7}, \quad |y_{\mu e}| \lesssim 2 \times 10^{-8}, \quad (5)$$

which severely limit any CLFV time-dependent effects that could arise at higher orders, via additional y_{ij} insertions.

3. *Mass-Shift Effects:* Setting ϕ in Eq. (4) to its background value ϕ_c yields corrections to the lepton mass matrix:

$$m_{ij}(t) = \text{diag}(m_e, m_\mu, m_\tau) + y_{ij}\phi_c(t), \quad (6)$$

where the additional mass terms induce time dependence in SM decays. For example, the branching ratio $\mathcal{B}(\mu \rightarrow e\nu\bar{\nu})$ acquires time modulation with an amplitude $\propto \mathcal{O}(y_{\mu\mu}, y_{\mu e}^2)$, due to the modified muon mass. Furthermore, these terms can also induce time-dependent exotic FCNC decays, such as $\mu \rightarrow e\gamma$ or $\tau \rightarrow e\gamma$. However, the branching fractions for these processes are suppressed by both y_{ij}^2 and by $\dot{\phi}_c$.² Thus, after taking into account the constraints from Eq. (5), all time-varying CLFV signals due to Eq. (4) are unobservably small.

² In the $\tau_\phi \gg \tau_\ell$ limit the ϕ_c term in Eq. (6) merely corrects the charged lepton mass matrix, and does not result in a new source of flavor violation.

To address these issues, one might consider an axion-like interaction of the form: $(\partial_\mu \phi) \bar{\ell}_i \gamma^\mu \gamma_5 \ell_j$, which solves problem (1) due to the ϕ shift symmetry, but does not address (2) or (3). Conversely, a non-linear Yukawa coupling of the form $\phi^2 \bar{\ell}_i \ell_j$ solves problems (2) and (3), but makes problem (1) much worse. In this case, quantum corrections to m_ϕ explicitly depend on the local DM density when ϕ_c is inserted into loop diagrams, requiring severe fine-tuning to maintain $m_\phi \ll \text{eV}$.

Thus, viably connecting the time-dependent DM background to flavor violating decays requires an interaction that both protects the scalar mass and couples ϕ non-linearly to the SM. The lowest dimension operator with these properties is

$$\mathcal{L}_{\text{int}} \supset \frac{i\phi(\partial_\mu \phi)}{2f^2} \bar{\ell}_i \gamma^\mu (C_{ij}^V + C_{ij}^A \gamma_5) \ell_j, \quad (7)$$

where $C_{ij}^{V,A}$ are hermitian matrices in flavor space and the i, j indices run over all charged fermion species and f is the energy scale associated with the generation of this operator. As we show in the Supplemental Material, the interaction in Eq. (7) can be the leading DM-SM interaction if ϕ is a pseudo-Nambu-Goldstone boson of a spontaneously broken non-Abelian global symmetry (in which case f is related to the scale of spontaneous symmetry breaking).

Since the interaction in Eq. (7) contains two ϕ insertions, expanding ϕ around its background value, ϕ_c , results in time-dependent FCNC decays at leading order. To make this time modulation manifest, we integrate by parts and replace one of the ϕ fields with ϕ_c to obtain

$$\mathcal{L}_{\text{int}} \supset \frac{\phi_c}{2f^2} \phi \bar{\ell}_i \left[C_{ij}^V (m_{\ell_i} - m_{\ell_j}) + C_{ij}^A (m_{\ell_i} + m_{\ell_j}) \gamma_5 \right] \ell_j, \quad (8)$$

where m_{ℓ_i} is the mass of ℓ_i . The branching fraction for $\ell_i \rightarrow \ell_j \phi$ decays is now explicitly time-dependent:

$$\mathcal{B}(\ell_i \rightarrow \ell_j \phi) = \frac{C_{ij}^2 \phi_0^2 m_{\ell_i}^3}{64\pi f^4 \Gamma_{\ell_i}} \cos^2(m_\phi t + \delta), \quad (9)$$

where $C_{ij}^2 \equiv |C_{ij}^V|^2 + |C_{ij}^A|^2$, Γ_{ℓ_i} is the total width of lepton ℓ_i , ϕ_0 is the field amplitude from Eq. (2), and we have approximated all final state particles as massless except for the appearance of m_ϕ in the cosine. Note that, as the dark matter candidate, ϕ must be cosmologically stable and, therefore, invisible on accelerator length scales.

Observing periodic signals. New physics transitions $\ell_i \rightarrow \ell_j \phi$ have an irreducible SM background from the tree-level W -boson mediated decays, $\ell_i \rightarrow \ell_j \nu_i \bar{\nu}_j$. Due to three-body kinematics, this background mimics the signal $\ell_i \rightarrow \ell_j \phi$ only when the invariant mass of the two neutrinos is close to zero, within experimental resolution (the ϕ mass is far below the invisible mass resolution in these experiments). Time-dependent signals offer a valuable handle to distinguish signal from background, particularly because the background events do not exhibit periodic modulation. Observing a time modulation

in $\ell_i \rightarrow \ell_j \phi$ decays would constitute compelling evidence for DM or another misaligned field with nontrivial cosmological abundance.³

We assess the statistical sensitivity to sinusoidal signals in Eq. (9) in the presence of substantial SM backgrounds using a simplified analysis. Assuming continuous data collection over total observation time T , the data are divided into $n_{\text{bin}} = T/\Delta t$ equal-sized bins, each of duration Δt , which are longer or equal to the experimental resolution. Using Eq. (9), the predicted event rate is

$$\dot{N}_{\text{pred}}(t) = \frac{N_{\text{tot}}}{T} [\mathcal{B}_{\text{bg}} f_{\text{bg}} + 2\mathcal{B}_{\text{sig}} f_{\text{sig}} \cos^2(m_\phi t + \delta)], \quad (10)$$

where N_{tot} is the total number of ℓ_i decays, $\mathcal{B}_{\text{bg}(\text{sig})}$ and $f_{\text{bg}(\text{sig})}$ are the background (signal) branching fractions and experimental efficiencies, respectively. Local DM with velocity $v \sim 10^{-3}$ sets a characteristic coherence time

$$\tau_{\text{coh}} \sim \frac{1}{m_\phi v^2} \simeq 7 \times 10^5 \text{ s} \left(\frac{10^{-15} \text{ eV}}{m_\phi} \right) \left(\frac{10^{-3}}{v} \right)^2, \quad (11)$$

during which the classical DM field maintains the same phase δ . For $T > \tau_{\text{coh}}$, an experiment can experience two or more coherent ‘patches’ with different phases. For more details about decoherence in our analysis, see the Supplemental Material [51]. In Eq. (10), the *time-averaged* branching ratio for the signal channel satisfies

$$\mathcal{B}_{\text{sig}} \equiv \langle \mathcal{B}(\ell_i \rightarrow \ell_j \phi) \rangle = \frac{C_{ij}^2 \phi_0^2 m_{\ell_i}^3}{128\pi f^4 \Gamma_{\ell_i}}, \quad (12)$$

where we have used Eq. (9). The number of background events, assumed to be non-modulating and dominant over the signal, is given by

$$N_{\text{bg}} = N_{\text{tot}} \mathcal{B}_{\text{bg}} f_{\text{bg}} \quad , \quad \mathcal{B}_{\text{bg}} f_{\text{bg}} \gg \mathcal{B}_{\text{sig}} f_{\text{sig}}. \quad (13)$$

The number of events per time bin is obtained from integrating $\dot{N}_{\text{pred}}(t)$ over each bin interval Δt . Using Asimov datasets⁴ we construct a χ^2 statistic test, which depends on the quadratic sum of statistical and systematic errors in each bin, which respectively satisfy

$$\sigma_{\text{stat}} = \sqrt{N_{\text{bg}}/n_{\text{bin}}}, \quad \sigma_{\text{sys}} = \alpha N_{\text{bg}}/n_{\text{bin}}, \quad (14)$$

where α is the relative systematic uncertainty. The χ^2 test statistic can then be translated to the expected bounds on $f/\sqrt{C_{ij}}$ from Eq. (9) using time-dependent $\ell_i \rightarrow \ell_j \phi$ searches. As shown in the Supplemental Material [51], in the ‘‘fine-binned’’ (fb) limit where $m_\phi \Delta t \ll 1$,

³ In general, ϕ could be a subdominant DM component, and still lead to a time-dependent signal.

⁴ In an Asimov data set, all observed quantities are set equal to their expected values.

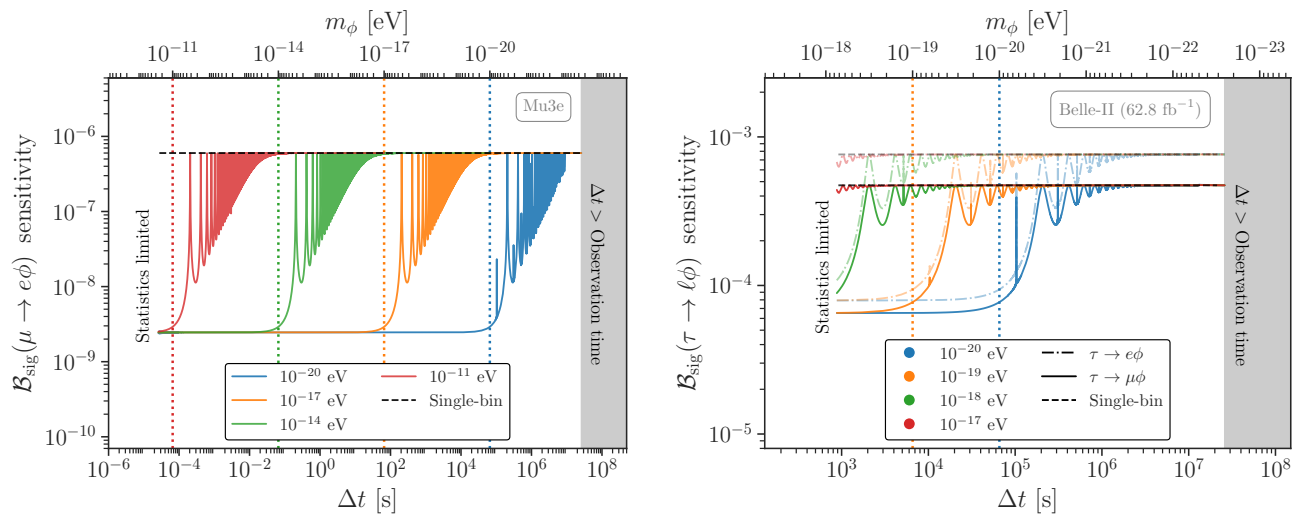


FIG. 2. The 90% confidence upper limit on the signal branching \mathcal{B}_{sig} obtained from a time-dependent analysis, as a function of bin size Δt (solid, dashed-dotted lines) for different ϕ masses at Mu3e (left) and Belle II (right), using the same assumptions as in Fig. 1. The dotted vertical lines denote approximately when the oscillatory signal for each mass is resolved, $\Delta t \sim m_\phi^{-1}$. The horizontal dashed black line denotes the upper limit for a time-independent, single-bin, analysis.

$m_\phi T \gg 1$, the time-dependent test statistic χ_{fb}^2 can be written

$$\chi_{\text{fb}}^2 = \frac{3}{2} \left[1 + \frac{n_{\text{bin}}}{3} \left(\frac{\sigma_{\text{sys}}}{\sigma_{\text{stat}}} \right)^2 \right] \chi_{\text{const}}^2, \quad (15)$$

where χ_{const}^2 is the usual time-independent test statistic. Thus, in the fine-binned limit, the sensitivity to a time-dependent signal is significantly enhanced if systematic uncertainties dominate over statistical ones. In fact, in the systematics-dominated regime, Eq. (15) reduces to [51]

$$\chi_{\text{fb}}^2 = \frac{(\mathcal{B}_{\text{sig}} f_{\text{sig}} N_{\text{tot}})^2}{2 n_{\text{bin}} \sigma_{\text{stat}}^2}, \quad (16)$$

which shows complete independence from systematic uncertainties. Thus, with an appropriate analysis, it is possible to measure a time-dependent signal even in the presence of large systematic uncertainties, as long as all the systematics are time-independent.

The expected sensitivity generally depends on the choice of time-bin width Δt (equivalently, the number of bins n_{bin}), as shown in Fig. 2. The time-independent limit corresponds to $n_{\text{bin}} = 1$ (dashed line in Fig. 2). Sensitivity gradually decreases as Δt increases: small Δt corresponds to a regime fully resolving oscillations, whereas large Δt approaches a less sensitive, time-integrated analysis dominated by systematics.

In Fig. 1, we summarize the expected sensitivity to $\mathcal{B}(l_i \rightarrow l_j \phi)$ as a function of m_ϕ for representative numerical examples detailed below. We choose the smallest feasible Δt (largest n_{bin}) consistent with valid χ^2 statistics, typically requiring at least ten events per time bin.

This choice consistently exceeds experimental time resolution in all examples. Further details on the procedure can be found in the Supplemental Material [51].

Numerical examples. As representative examples we consider a possible search for time-dependent $\mu \rightarrow e\phi$ decays at Mu3e, and for $\tau \rightarrow \ell\phi$ decays at Belle II and at FCC-ee. More details regarding the chosen numerical values for each example can be found in the Supplemental Material [51].

For Mu3e, we assume $T = 300$ days of continuous data collection, yielding $N_{\text{tot}} \sim 3 \times 10^{15}$ muon decays. The endpoint region for $m_\phi \simeq 0$ includes $N_{\text{bg}} \sim 10^{13}$ background events from $\mu \rightarrow e\nu\bar{\nu}$, corresponding to a background fraction $f_{\text{bg}} \sim 3 \times 10^{-3}$ [27, 28]. For these large data samples, the $\mu \rightarrow e\phi$ search will be dominated by systematics, which we conservatively assume are set by theoretical uncertainties, implying a 90% CL upper bound of $\mathcal{B}(\mu \rightarrow e\phi) < 6 \times 10^{-7}$ (Fig. 12 of Ref. [52]), and thus a relative systematic uncertainty of $\alpha \sim 10^{-4}$. Given the dataset above, the time-dependent search for $\mu \rightarrow e\phi$ can result in a sensitivity to the $\mu \rightarrow e\phi$ branching ratio well below the systematic uncertainty for $m_\phi \lesssim 10^{-10}$ eV (solid purple line in Fig. 1 left).

Estimating the Belle-II sensitivity to time-dependent $\tau \rightarrow \ell\phi$ decays is complicated by the fact that the state-of-the-art time-integrated search for these decays relies on the combined fit to the shape of $\tau \rightarrow \ell\nu\bar{\nu}$ background and the $\tau \rightarrow \ell\phi$ signal in the pseudo-rest-frame of the tau [25]. Since, in this frame, the spectrum of lepton energies in SM $\tau \rightarrow \ell\nu\bar{\nu}$ decays is similar to the spectrum from $\tau \rightarrow \ell\phi$, we approximate the sensitivity using a simplified counting experiment. For the existing Belle-II analysis [25], using data corresponding to an integrated luminosity of 62.8 fb^{-1} , we consider only the

$\tau \rightarrow \ell\nu\bar{\nu}$ events with lepton energies in the range that contains 90% of the signal leptons from $\tau \rightarrow \ell\phi$ decays. Taking experimental efficiencies into account gives $f_{\text{sig}}^{e[\mu]} \sim 0.12[0.16]$ and $f_{\text{bg}}^{e[\mu]} \sim 8[9] \times 10^{-2}$. Using this, the background process branching $\mathcal{B}_{\text{bg}}^{e[\mu]} \sim 3 \times 10^{-2}$, the 90% CL upper limits set by the analysis $B(\tau \rightarrow e[\mu]\phi) < 7.6[4.7] \times 10^{-4}$ [25], and assuming that the search is systematics limited, gives the relative systematic uncertainty of $\alpha_{e[\mu]} \sim 6[4] \times 10^{-2}$. For simplicity, we also assume that the $N_{\text{tot}} \sim 10^8$ taus were collected uniformly within $T = 300$ days. Using this relatively small data-sample, the time-dependent search resolves oscillations only for ϕ masses below $m_\phi \lesssim 10^{-17}$ eV (blue solid line in Fig. 1 right). With the full 50 ab^{-1} integrated luminosity, Belle-II will have $N_{\text{tot}} \sim 10^{11}$, which should significantly improve the reach in $f^2/C_{\tau\ell}$ and sensitivity to larger ϕ masses. Assuming continuous data collection over $T = 3 \times 10^3$ days with unchanged f_{bg} , f_{sig} , and α , yields the blue dashed-dotted line in Fig. 1 (right).

Finally, we also consider $\tau \rightarrow \ell\phi$ searches at FCC-ee. While running in Tera-Z mode the proposed FCC-ee experiment will produce approximately $N_{\text{tot}} = 3.4 \times 10^{11}$ taus over $T = 740$ days of running [30]. Using a relative systematic uncertainty of $\alpha \sim 1.7 \times 10^{-3}$, $f_{\text{bg}} \sim 0.5$, and $f_{\text{sig}} \sim 0.8$ we obtain the projected sensitivities shown as the red solid line in Fig. 1 (right), resolving oscillations up to $m_\phi \lesssim 10^{-13}$ eV.

Astrophysical and laboratory constraints. Light particles with CFLV interactions can modify energy transport in supernovae and conflict with the observed properties of SN1987A in the Large Magellanic Cloud (LMC) [33]. Previous bounds on such particles assumed environment-independent couplings, but our interaction from Eq. (8) depends on ϕ_c and thus requires knowledge of the DM density in the LMC. At the SN1987A location (~ 1 kpc from the LMC center [53]), the DM density is estimated to be [54]

$$\rho_\phi^{\text{LMC}} \in [0.4, 8] \text{ GeV/cm}^3, \quad (17)$$

and in Fig. 1 (left) we use the lower end of this range to place conservative limits on the quantity $f/\sqrt{C_{\mu e}}$, following the same procedure as outlined in Ref. [55].

It is instructive to compare CLFV constraints to those on flavor-diagonal couplings. As diagonal scalar couplings vanish in our model at leading order, see Eq. (8), we consider constraints on an ultralight pseudoscalar DM and define $C_{\mu e}|_{\text{Mu3e}}$ as the maximum Mu3e sensitivity in Fig. 1, reflecting a time-binned analysis with fine binning. The strongest constraints on the diagonal electron couplings are from Red Giant cooling [56]

$$C_{ee} \left(\frac{\text{GeV}}{f} \right)^2 \lesssim 2 \times 10^2 \left(\frac{m_\phi}{\text{eV}} \right), \quad (18)$$

while for the diagonal muon coupling, the strongest con-

straints come from SN1987A cooling, where [57, 58]

$$C_{\mu\mu} \left(\frac{\text{GeV}}{f} \right)^2 \lesssim 8 \times 10^4 \left(\frac{m_\phi}{\text{eV}} \right), \quad (19)$$

which yields the relations

$$C_{ee} \lesssim 30 C_{\mu e}|_{\text{Mu3e}}, \quad C_{\mu\mu} \lesssim 10^4 C_{\mu e}|_{\text{Mu3e}}. \quad (20)$$

Without fine-tuned cancellations, rotating into the charged-lepton mass basis generally produces

$$C_{\mu e} \lesssim \sqrt{C_{ee} C_{\mu\mu}} \lesssim 5 \times 10^2 C_{\mu e}|_{\text{Mu3e}} \quad (21)$$

where we have combined Eqs. (18)–(20) in the last expression. This indicates that Mu3e searches can probe new and *natural* DM parameter space without special hierarchies between diagonal and off-diagonal couplings. Given the much weaker bounds on $C_{\tau\tau}$, the Belle-II searches we describe above also do not face any such fine-tuning considerations, especially for $\tau \rightarrow \mu\phi$ decays.

Conclusions. In this *Letter* we demonstrated that FCNC decays may offer a new window into ultralight DM candidates. Crucially, the presence of FCNC couplings to charged SM leptons can induce time modulation in $\tau \rightarrow \ell\phi$ and $\mu \rightarrow e\phi$ decays, where ϕ is the DM field. Since observing time dependence in these decays would be smoking-gun evidence of DM, we find that rare lepton decay experiments can also serve as potential dark matter direct detection experiments without any instrumental modifications. Furthermore, such time-oscillating signals can improve the experimental reach compared to time-independent searches, if the latter are dominated by systematic uncertainties, see Fig. 1.

While our analysis focused on flavor violation in charged lepton decays, the same approach directly extends both to other observables in the lepton sector (such as $\mu \rightarrow e$ conversion in the field of a nucleus), as well as to flavor violation in the quark sector. We leave a more detailed analysis of these phenomena for future work.

ACKNOWLEDGMENTS

We are indebted to Joachim Kopp for physics discussions during the early stages of this work. This manuscript has been authored in part by Fermi Forward Discovery Group, LLC under Contract No. 89243024CSC000002 with the U.S. Department of Energy, Office of Science, Office of High Energy Physics. The work of IB, PF and RH was performed in part at the Aspen Center for Physics, supported by a grant from the Alfred P. Sloan Foundation (G-2024-22395). YG acknowledges support by the Cluster of Excellence ‘‘PRISMA+’’ funded by the German Research Foundation (DFG) within the German Excellence Strategy (Project No. 390831469), and by a fellowship awarded by the Azrieli Foundation. JZ and TM acknowledge support in part by the DOE grant de-sc0011784, and NSF grants OAC-2103889, OAC-2411215, and OAC-2417682. JZ and TM also acknowledge support in part from the Visiting Scholars Award Program of the Universities Research Association.

-
- [1] M. Cirelli, A. Strumia, and J. Zupan, (2024), arXiv:2406.01705 [hep-ph].
- [2] P. Ilten *et al.*, in *Snowmass 2021* (2022) arXiv:2206.04220 [hep-ex].
- [3] Y. Kahn and T. Lin, *Rept. Prog. Phys.* **85**, 066901 (2022), arXiv:2108.03239 [hep-ph].
- [4] A. Mitridate, T. Trickle, Z. Zhang, and K. M. Zurek, *Phys. Dark Univ.* **40**, 101221 (2023), arXiv:2203.07492 [hep-ph].
- [5] J. Jaeckel, G. Rybka, and L. Winslow, (2022), arXiv:2209.08125 [hep-ph].
- [6] S. Tremaine and J. E. Gunn, *Phys. Rev. Lett.* **42**, 407 (1979).
- [7] M. S. Turner, *Phys. Rev. D* **28**, 1243 (1983).
- [8] P. F. de Salas and A. Widmark, *Rept. Prog. Phys.* **84**, 104901 (2021), arXiv:2012.11477 [astro-ph.GA].
- [9] T. Zimmermann, J. Alvey, D. J. E. Marsh, M. Fairbairn, and J. I. Read, (2024), arXiv:2405.20374 [astro-ph.CO].
- [10] M. Benito, G. Hütsi, K. Müürsepp, J. Sánchez-Almeida, J. Urrutia, V. Vaskonen, and H. Veermäe, (2025), arXiv:2502.12030 [astro-ph.CO].
- [11] D. Antypas *et al.*, (2022), arXiv:2203.14915 [hep-ex].
- [12] L. Hui, *Ann. Rev. Astron. Astrophys.* **59**, 247 (2021), arXiv:2101.11735 [astro-ph.CO].
- [13] M. S. Safronova, D. Budker, D. DeMille, D. F. J. Kimball, A. Derevianko, and C. W. Clark, *Rev. Mod. Phys.* **90**, 025008 (2018), arXiv:1710.01833 [physics.atom-ph].
- [14] A. Berlin, *Phys. Rev. Lett.* **117**, 231801 (2016), arXiv:1608.01307 [hep-ph].
- [15] V. Brdar, J. Kopp, J. Liu, P. Prass, and X.-P. Wang, *Phys. Rev. D* **97**, 043001 (2018), arXiv:1705.09455 [hep-ph].
- [16] G. Krnjaic, P. A. N. Machado, and L. Necib, *Phys. Rev. D* **97**, 075017 (2018), arXiv:1705.06740 [hep-ph].
- [17] F. Capozzi, I. M. Shoemaker, and L. Vecchi, *JCAP* **07**, 004 (2018), arXiv:1804.05117 [hep-ph].
- [18] A. Dev, G. Krnjaic, P. Machado, and H. Ramani, *Phys. Rev. D* **107**, 035006 (2023), arXiv:2205.06821 [hep-ph].
- [19] M. Losada, Y. Nir, G. Perez, I. Savoray, and Y. Shpilman, *Phys. Rev. D* **108**, 055004 (2023), arXiv:2302.00005 [hep-ph].
- [20] M. Dine, G. Perez, W. Ratzinger, and I. Savoray, (2024), arXiv:2405.06744 [hep-ph].
- [21] D. Lee, U.-G. Meißner, K. A. Olive, M. Shifman, and T. Vonk, *Phys. Rev. Res.* **2**, 033392 (2020), arXiv:2006.12321 [hep-ph].
- [22] X. Zhang, N. Houston, and T. Li, *Phys. Rev. D* **108**, L071101 (2023), arXiv:2303.09865 [hep-ph].
- [23] J. Alda, C. Brogini, G. Di Carlo, L. Di Luzio, D. Piatti, S. Rigolin, and C. Toni, (2024), arXiv:2412.20932 [hep-ph].
- [24] W. Altmannshofer *et al.* (Belle-II), *PTEP* **2019**, 123C01 (2019), [Erratum: *PTEP* 2020, 029201 (2020)], arXiv:1808.10567 [hep-ex].
- [25] I. Adachi *et al.* (Belle-II), *Phys. Rev. Lett.* **130**, 181803 (2023), arXiv:2212.03634 [hep-ex].
- [26] K. Arndt *et al.* (Mu3e), *Nucl. Instrum. Meth. A* **1014**, 165679 (2021), arXiv:2009.11690 [physics.ins-det].
- [27] A.-K. Perrevoort, *Ph.D. thesis*, U. Heidelberg (main) (2018).
- [28] A.-K. Perrevoort (Mu3e), *Phys. Sci. Forum* **8**, 30 (2023), arXiv:2308.11403 [hep-ex].
- [29] A. Abada *et al.* (FCC), *Eur. Phys. J. C* **79**, 474 (2019).
- [30] G. Bernardi *et al.*, (2022), arXiv:2203.06520 [hep-ex].
- [31] M. Dam, *SciPost Phys. Proc.* **1**, 041 (2019), arXiv:1811.09408 [hep-ex].
- [32] A. M. Baldini *et al.* (MEG II), *Eur. Phys. J. C* **78**, 380 (2018), arXiv:1801.04688 [physics.ins-det].
- [33] L. Calibbi, D. Redigolo, R. Ziegler, and J. Zupan, *JHEP* **09**, 173 (2021), arXiv:2006.04795 [hep-ph].
- [34] Y. Jho, S. Knapen, and D. Redigolo, *JHEP* **10**, 029 (2022), arXiv:2203.11222 [hep-ph].
- [35] R. M. Carey *et al.* (Mu2e), (2008), 10.2172/952028.
- [36] L. Bartoszek *et al.* (Mu2e), (2014), 10.2172/1172555, arXiv:1501.05241 [physics.ins-det].
- [37] R. H. Bernstein (Mu2e), *Front. in Phys.* **7**, 1 (2019), arXiv:1901.11099 [physics.ins-det].
- [38] R. J. Hill, R. Plestid, and J. Zupan, *Phys. Rev. D* **109**, 035025 (2024), arXiv:2310.00043 [hep-ph].
- [39] S. Knapen, K. Langhoff, T. Opferkuch, and D. Redigolo, (2023), arXiv:2311.17915 [hep-ph].
- [40] R. Abramishvili *et al.* (COMET), *PTEP* **2020**, 033C01 (2020), arXiv:1812.09018 [physics.ins-det].
- [41] Y. Kuno (COMET), *PTEP* **2013**, 022C01 (2013).
- [42] M. Ablikim *et al.* (BESIII), *Chin. Phys. C* **44**, 040001 (2020), arXiv:1912.05983 [hep-ex].
- [43] M. Ablikim *et al.* (BESIII), *Nucl. Instrum. Meth. A* **614**, 345 (2010), arXiv:0911.4960 [physics.ins-det].
- [44] A. Pich, *Int. J. Mod. Phys. A* **39**, 2442002 (2024), arXiv:2405.19955 [hep-ph].
- [45] M. N. Achasov *et al.*, *Phys. Usp.* **vol**, 55 (2024).
- [46] M. Achasov *et al.*, *Front. Phys. (Beijing)* **19**, 14701 (2024), arXiv:2303.15790 [hep-ex].
- [47] X. Ai *et al.*, (2024), arXiv:2412.19743 [hep-ex].
- [48] J. R. Musser *et al.* (TWIST), *Phys. Rev. Lett.* **94**, 101805 (2005), arXiv:hep-ex/0409063.
- [49] G. G. Raffelt, *Phys. Rept.* **198**, 1 (1990).
- [50] A. Jodidio *et al.*, *Phys. Rev. D* **34**, 1967 (1986), [Erratum: *Phys.Rev.D* 37, 237 (1988)].
- [51] see Supplemental Material.
- [52] P. Banerjee, A. M. Coutinho, T. Engel, A. Gurgone, A. Signer, and Y. Ulrich, (2022), arXiv:2211.01040 [hep-ph].
- [53] N. Panagia, R. Gilmozzi, F. Macchetto, H. M. Adorf, and R. P. Kirshner, *Astrop. J. Lett.* **380**, L23 (1991).
- [54] M. R. Buckley, E. Charles, J. M. Gaskins, A. M. Brooks, A. Drlica-Wagner, P. Martin, and G. Zhao, *Phys. Rev. D* **91**, 102001 (2015), arXiv:1502.01020 [astro-ph.HE].
- [55] L. Calibbi, F. Goertz, D. Redigolo, R. Ziegler, and J. Zupan, *Phys. Rev. D* **95**, 095009 (2017), arXiv:1612.08040 [hep-ph].
- [56] F. Capozzi and G. Raffelt, *Phys. Rev. D* **102**, 083007 (2020), arXiv:2007.03694 [astro-ph.SR].

- [57] R. Bollig, W. DeRocco, P. W. Graham, and H.-T. Janka, *Phys. Rev. Lett.* **125**, 051104 (2020), [Erratum: *Phys.Rev.Lett.* 126, 189901 (2021)], [arXiv:2005.07141 \[hep-ph\]](#).
- [58] A. Caputo, G. Raffelt, and E. Vitagliano, *Phys. Rev. D* **105**, 035022 (2022), [arXiv:2109.03244 \[hep-ph\]](#).
- [59] R. D. Peccei and H. R. Quinn, *Phys. Rev. Lett.* **38**, 1440 (1977).
- [60] R. D. Peccei and H. R. Quinn, *Phys. Rev. D* **16**, 1791 (1977).
- [61] F. Wilczek, *Phys. Rev. Lett.* **40**, 279 (1978).
- [62] S. Weinberg, *Phys. Rev. Lett.* **40**, 223 (1978).
- [63] J. F. Donoghue, E. Golowich, and B. R. Holstein, *Dynamics of the standard model*, Vol. 2 (CUP, 2014).
- [64] Y. Hochberg, E. Kuflik, H. Murayama, T. Volansky, and J. G. Wacker, *Phys. Rev. Lett.* **115**, 021301 (2015), [arXiv:1411.3727 \[hep-ph\]](#).
- [65] Y. Hochberg, E. Kuflik, and H. Murayama, *JHEP* **05**, 090 (2016), [arXiv:1512.07917 \[hep-ph\]](#).
- [66] S.-M. Choi, Y. Hochberg, E. Kuflik, H. M. Lee, Y. Mambrini, H. Murayama, and M. Pierre, *JHEP* **10**, 162 (2017), [arXiv:1707.01434 \[hep-ph\]](#).
- [67] Y. Hochberg, E. Kuflik, R. McGehee, H. Murayama, and K. Schutz, *Phys. Rev. D* **98**, 115031 (2018), [arXiv:1806.10139 \[hep-ph\]](#).
- [68] Y. Hochberg, E. Kuflik, and H. Murayama, *Phys. Rev. D* **99**, 015005 (2019), [arXiv:1805.09345 \[hep-ph\]](#).
- [69] G. Krnjaic and K. Sigurdson, *Phys. Lett. B* **751**, 464 (2015), [arXiv:1406.1171 \[hep-ph\]](#).
- [70] R. Balkin, M. Ruhdorfer, E. Salvioni, and A. Weiler, *JCAP* **11**, 050 (2018), [arXiv:1809.09106 \[hep-ph\]](#).
- [71] R. Balkin, G. Perez, and A. Weiler, *Eur. Phys. J. C* **78**, 104 (2018), [arXiv:1707.09980 \[hep-ph\]](#).
- [72] D. Marzocca and A. Urbano, *JHEP* **07**, 107 (2014), [arXiv:1404.7419 \[hep-ph\]](#).
- [73] M. Frigerio, A. Pomarol, F. Riva, and A. Urbano, *JHEP* **07**, 015 (2012), [arXiv:1204.2808 \[hep-ph\]](#).
- [74] A. Berlin, N. Blinov, S. Gori, P. Schuster, and N. Toro, *Phys. Rev. D* **97**, 055033 (2018), [arXiv:1801.05805 \[hep-ph\]](#).
- [75] E. Bernreuther, F. Kahlhoefer, M. Krämer, and P. Tunney, *JHEP* **01**, 162 (2020), [arXiv:1907.04346 \[hep-ph\]](#).
- [76] G. D. Kribs, A. Martin, B. Ostdiek, and T. Tong, *JHEP* **07**, 133 (2019), [arXiv:1809.10184 \[hep-ph\]](#).
- [77] S. Renner and P. Schwaller, *JHEP* **08**, 052 (2018), [arXiv:1803.08080 \[hep-ph\]](#).
- [78] J. F. Eguren, S. Klingel, E. Stamou, M. Tabet, and R. Ziegler, *JHEP* **08**, 111 (2024), [arXiv:2405.00108 \[hep-ph\]](#).
- [79] J. T. VanderPlas, *The Astrophysical Journal Supplement Series* **236**, 16 (2018).
- [80] S. Navas *et al.* (Particle Data Group), *Phys. Rev. D* **110**, 030001 (2024).
- [81] M. G. Hernandez, *Search for new physics in charged lepton flavor violating processes at the Belle II experiment.*, Ph.D. thesis, Cinvestav-IPN, CINVESTAV, IPN (2023).
- [82] E. De La Cruz-Burelo, M. Hernandez-Villanueva, and A. De Yta-Hernandez, *Phys. Rev. D* **102**, 115001 (2020), [arXiv:2007.08239 \[hep-ph\]](#).
- [83] M. Dam, *Eur. Phys. J. Plus* **136**, 963 (2021).

SUPPLEMENTAL MATERIAL

1. Non-Abelian pseudo-NGBs

A spontaneously broken global symmetry gives rise to massless Nambu-Goldstone Bosons (NGBs). The NGBs acquire a nonzero mass if there is a small explicit breaking of the global symmetry. Celebrated examples of NGBs in particle physics are the QCD axion, and the light mesons π^\pm and π^0 . The QCD axion is a pseudo-NGB of a $U(1)_{\text{PQ}}$ Peccei-Quinn global symmetry, spontaneously broken at high scale f_a and then also explicitly broken by the QCD anomaly [59–62]. The pions are the NGBs of spontaneous chiral symmetry breaking in QCD, $SU(2)_L \times SU(2)_R \rightarrow SU(2)_V$, where the initial $SU(2)_L \times SU(2)_R$ global group is also explicitly broken by the $m_{u,d}$ quark masses (see, e.g., [63]). The QCD axion is an example of an Abelian pNGB, while the pions are examples of non-Abelian pNGBs.

More generally, the non-Abelian pseudo-Goldstone Bosons (npNGBs) arise when the theory is invariant under an approximate non-Abelian global group G , that is spontaneously broken to its subgroup H ($G \rightarrow H$), where the G/H coset consists of several pNGBs that have non-linear interactions with each other. Let us denote the npNGB parametrization of the G/H coset as $U(\phi)$ where, under G transformations, $U(\phi) \rightarrow V_L^\dagger U(\phi) V_R$. In general, the left and right transformations differ so that $V_L \neq V_R$; this is the case we are interested in.⁵ The leading low-energy interaction Lagrangian between the npNGB dark sector and the SM, invariant under the symmetry group G , is then given by

$$\mathcal{L}_{\text{int}} \supset \text{Tr} (U^\dagger i \partial_\mu U) \bar{\ell}_i \gamma^\mu (\tilde{C}_{\ell_i \ell_j}^V + \tilde{C}_{\ell_i \ell_j}^A \gamma_5) \ell_j + \text{h.c.}, \quad (\text{S1})$$

where ℓ_i are the SM charged leptons. The above interaction would, for instance, be generated after heavy mediators are integrated out, but variants of this model with light mediators can also be considered.

Expanding the $U(\phi)$ exponentiation in terms of the ϕ_a fields gives dimension-6 interaction operators,

$$\mathcal{L}_{\text{int}} \supset \sum_a \frac{\phi_a}{f} \frac{i \partial_\mu \phi_a}{2f} \bar{\ell}_i \gamma^\mu (C_{\ell_i \ell_j}^V + C_{\ell_i \ell_j}^A \gamma_5) \ell_j, \quad (\text{S2})$$

where f is the scale of spontaneous symmetry breaking. We linearly transform ϕ_a such that the dark sector currents do not change the ϕ_a species, while the flavor structure of the SM currents is kept completely general. We recover Eq. (7) in the main text if only one of the ϕ_a fields is the DM, but Eq. (S2) also generalizes this to a multi-component DM scenario. In the framework of Eq. (S2), in the absence of additional sources of symmetry breaking, dark matter will be multi-component and consist equally of each component of the multiplet ϕ_a . Introducing additional soft sources of symmetry breaking leads to only a subset of the multiplet identified as dark matter – possibly only a single component.

The above structure of interactions in Eq. (S1) may seem exotic. However, as noted above, there is a familiar example in the SM: the pion sector of QCD interacting through QED with leptons. The spontaneous breaking of chiral symmetry in QCD, $SU(2)_L \otimes SU(2)_R \rightarrow SU(2)_V$ results in three light npNGBs, π^\pm and π^0 . The $\pi^+ i \partial_\mu \pi^-$ current couples to the electromagnetic current of the SM leptons through a tree level photon exchange, giving rise to a non-local interaction of the form $(\pi^+ i \partial_\mu \pi^-) \partial^{-2} (\bar{\ell} \gamma^\mu \ell)$, where the nonlocal structure ∂^{-2} is due to the photon propagator, $-i g_{\mu\nu}/q^2$, but in the position-space representation.

These npNGBs have also been discussed in the literature as the possible dark matter candidates. An example is the strongly interacting massive particle (SIMP) dark matter candidate [64–68]. While in the SIMP case the interesting mass regime is around GeV, we are interested in much lighter npNGB dark matter candidates, with masses well below eV. For other examples of heavier npNGB dark matter, see, e.g., Refs. [69–73], and for strongly-interacting dark sectors with dark pions as npNGBs, see, e.g., Refs. [74–77]. The dark sector currents of the form $\phi \partial_\mu \phi$ coupling to SM fermion currents through light dark vectors were also considered in [78].

In QCD the π^0 has an anomaly induced coupling to photons of the form $\pi^0 F \tilde{F}$. The same can be true of the dark sector npNGBs, which can also have dimension-5 anomaly-like interaction terms with the SM gauge bosons

$$\mathcal{L}_{\text{int}} \supset c_g^a \frac{\phi_a}{f} \frac{\alpha_s}{8\pi} G_{\mu\nu}^\beta \tilde{G}^{\beta\mu\nu} + c_\gamma^a \frac{\phi_a}{f} \frac{\alpha_{\text{em}}}{8\pi} F_{\mu\nu} \tilde{F}^{\mu\nu}. \quad (\text{S3})$$

⁵ If $V_L = V_R$, then $\text{Tr} \partial_\mu U \sim \partial_\mu \phi_a$ is invariant under G . At low energies, interactions of the form $\partial \phi_a \bar{\ell}_i \gamma^\mu \ell_j$ are then also allowed – i.e., the same interaction types that are generally present for

a QCD axion, or any other $U(1)$ pNGB. We define non-Abelian pNGBs to be the models where such terms are absent, although one could also consider the case where both Abelian and non-Abelian terms are present.

If there is no dark sector–SM mixed anomaly, however, the couplings c_g^a, c_γ^a will be proportional to the explicit breaking of the global shift symmetry, and thus may be highly suppressed, depending on the symmetry structure of the theory.

It is illuminating to compare the phenomenology of the FCNCs $\ell_i \rightarrow \ell_j \phi$ decays for the two cases, when ϕ is a non-Abelian pNGB, and when ϕ is an Abelian pNGB. For non-Abelian pNGBs the $\ell_i \rightarrow \ell_j \phi$ decays are induced by interaction in Eq. (7), while for Abelian pNGBs the interaction involves only a single ϕ field,

$$\mathcal{L} \supset C_{\ell_i \ell_j} \left(\frac{\partial_\mu \phi}{f} \right) \bar{\ell}_i \gamma^\mu \gamma_5 \ell_j. \quad (\text{S4})$$

There are several important differences between the two cases. First of all, since the interaction in Eq. (S4) is linear in ϕ , the $\ell_i \rightarrow \ell_j \phi$ decay rates for Abelian pNGB case are time independent, and also do not depend on the local DM number density. In contrast, for npNGBs the two-body $\ell_i \rightarrow \ell_j \phi$ decays arise only, if there is a background density of light ϕ particles. This background density then leads to time-dependent $\ell_i \rightarrow \ell_j \phi$ rates. The observation of such time-dependent $\ell_i \rightarrow \ell_j \phi$ decays would be a smoking-gun signal of light npNGB dark matter. For Abelian pNGB the observation of $\ell_i \rightarrow \ell_j \phi$ signal instead does not immediately imply that ϕ is DM, and one would need to confirm that ϕ is indeed the DM using other observations (for instance by searching for time-dependent interactions via its couplings to electrons).

2. Time-dependent χ^2 analysis

Here we present the details necessary to estimate the time-dependent sensitivity projection for the sinusoidal $\ell_i \rightarrow \ell_j \phi$ signal from Eq. (9). To simplify the analysis we consider an idealized case: an experiment that can collect data continuously for a total observation time $T > \tau_\phi$, with a constant time resolution $\Delta t < \tau_\phi$, and with a constant efficiency close to unity. In a realistic experimental analysis these simplifying assumptions may not be realized, implications of which we will discuss in Sec. 2d.

Since galactic DM is non-relativistic with local velocity $\mathcal{O}(v) \sim 10^{-3}$, its energy spread is $\mathcal{O}(v^2) \sim 10^{-6}$, so the the signal in Eq. (9) is coherent over $\mathcal{O}(10^6)$ oscillations. Therefore, in our analysis we separately consider two cases:

1. **Coherent (“slow”) oscillations:** for sufficiently slow oscillations, we can assume that the signal is coherent over the complete data collection time, which we discuss in Sec. 2a,
2. **Incoherent (“fast”) oscillations:** for faster oscillations we need to take into account the random phase variations using δ in Eq. (9), as discussed in Sec. 2b.

The time-integrated analysis is given in Sec. 2c.

a. Coherent (“slow”) oscillations

We first consider time-oscillating $\ell_i \rightarrow \ell_j \phi$ decays with a fixed phase. To estimate the expected upper bound on the branching ratio of the oscillating signal, we construct a χ^2 test statistic, and work with the “Asimov” data set, which assumes that each of the $n_{\text{bin}} = T/\Delta t$ bins will contain the “predicted” event counts (N_{pred}) under a given hypothesis. Since background processes are assumed not to oscillate, the expected number of background events is taken to be constant in each bin. Thus, in the presence of the oscillatory signal from Eq. (10) with fixed phase δ , the total number of predicted number of events in k^{th} time bin, with $t \in [t_{k-1}, t_k]$, is given by

$$N_{\text{pred},k} = \int_{t_{k-1}}^{t_k} dt \dot{N}_{\text{pred}} = \frac{N_{\text{tot}}}{T} \int_{t_{k-1}}^{t_k} dt [\mathcal{B}_{\text{bg}} f_{\text{bg}} + 2\mathcal{B}_{\text{sig}} f_{\text{sig}} \cos^2(m_\phi t + \delta)], \quad (\text{S5})$$

where N_{tot} is the total number of observed ℓ_i decays, \mathcal{B}_{sig} (\mathcal{B}_{bg}) is the $\ell_i \rightarrow \ell_j \phi$ ($\ell_i \rightarrow \ell_j \nu \bar{\nu}$) *time-averaged* branching ratio, while $f_{\text{sig(bg)}}$ is the experimental efficiency – which includes both detection efficiencies and experimental cuts. As anticipated, under the background-only hypothesis, the expected number of observed events is constant across all bins, so

$$N_{\text{bg},1} \equiv N_{\text{pred},k} \Big|_{\mathcal{B}_{\text{sig}} \rightarrow 0} = N_{\text{tot}} \mathcal{B}_{\text{bg}} f_{\text{bg}} \left(\frac{\Delta t}{T} \right), \quad (\text{S6})$$

where we have defined $N_{\text{bg},1}$ to be the constant background count in each bin. In the limit of large backgrounds, we take the statistical uncertainty in each bin to satisfy $\sigma_{\text{stat}}^2 = N_{\text{bg},1}$, consistent with the use of the Asimov set. We also

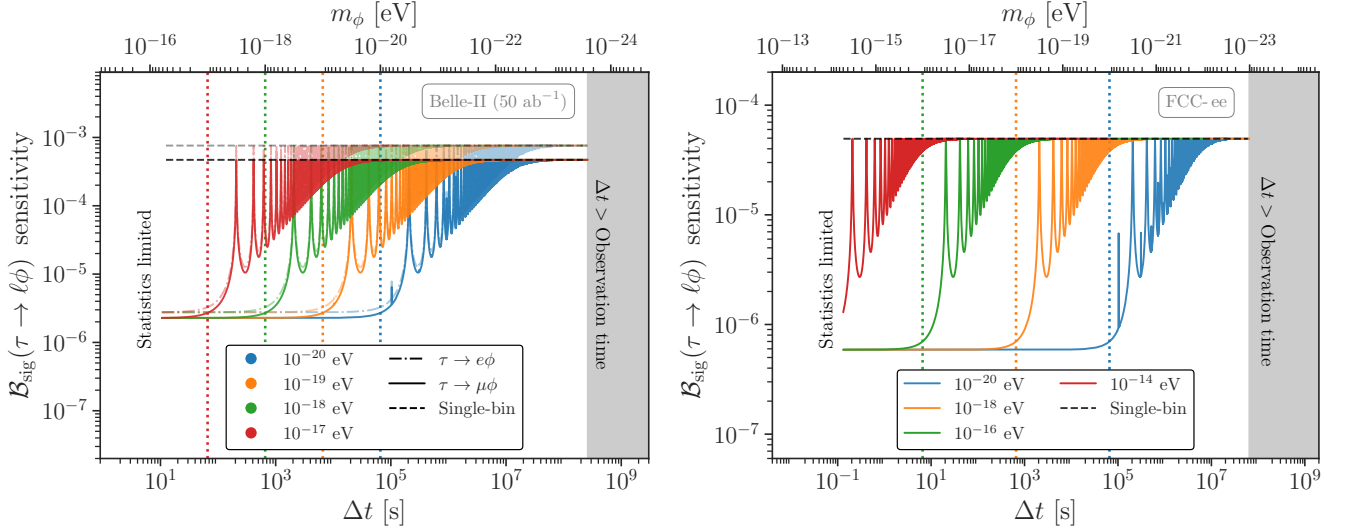


FIG. 3. Same as Fig. 2 for the full integrated luminosity at Belle-II (left) as well the projection for FCC-ee (right).

take into account systematic uncertainties, modeled by $\sigma_{\text{sys}}^2 = \alpha^2 N_{\text{bg},1}^2$ with α common to all bins – i.e., we assume that the systematic error is a fixed, time-independent, relative error. Therefore, systematics are fully correlated across all time bins, and the covariance matrix and its inverse are given by

$$C = N_{\text{bg},1} \mathbf{1} + \alpha^2 N_{\text{bg},1}^2 \mathbb{I}, \quad \text{and} \quad C^{-1} = \frac{1}{N_{\text{bg},1}} \mathbf{1} - \frac{\alpha^2}{1 + \alpha^2 N_{\text{bg},1} n_{\text{bin}}} \mathbb{I}, \quad (\text{S7})$$

where $\mathbf{1}$ is the $n_{\text{bin}} \times n_{\text{bin}}$ identity matrix and \mathbb{I} is the $n_{\text{bin}} \times n_{\text{bin}}$ constant unity matrix with 1 in every entry. The corresponding χ^2 statistic is therefore given by

$$\chi^2 = \sum_{k,p=1}^{n_{\text{bin}}} S_k C_{kp}^{-1} S_p = \frac{1}{N_{\text{bg},1}} \sum_{k=1}^{n_{\text{bin}}} S_k^2 - \frac{\alpha^2}{1 + \alpha^2 n_{\text{bin}} N_{\text{bg},1}} \left(\sum_{k=1}^{n_{\text{bin}}} S_k \right)^2, \quad (\text{S8})$$

where $S_k \equiv N_{\text{obs}}^k - N_{\text{pred}}^k$ is the number of signal events in bin k . For the signal in Eq. (S5) we then have

$$\begin{aligned} S_k &= 2\mathcal{B}_{\text{sig}} f_{\text{sig}} \frac{N_{\text{tot}}}{T} \int_{(k-1)\Delta t}^{k\Delta t} dt \cos^2(m_\phi t + \delta) \\ &= \mathcal{B}_{\text{sig}} f_{\text{sig}} \frac{N_{\text{tot}}}{T} \left[\Delta t + \frac{\sin(2km_\phi\Delta t + 2\delta) - \sin(2(k-1)m_\phi\Delta t + 2\delta)}{2m_\phi} \right], \end{aligned} \quad (\text{S9})$$

so using this expression, the two terms in the χ^2 in Eq. (S8) can be computed explicitly, and satisfy

$$\sum_{k=1}^{n_{\text{bin}}} S_k = \mathcal{B}_{\text{sig}} f_{\text{sig}} N_{\text{tot}} \left[1 + \frac{\sin(2m_\phi T + 2\delta) - \sin(2\delta)}{2m_\phi T} \right], \quad (\text{S10})$$

$$\begin{aligned} \sum_{k=1}^{n_{\text{bin}}} S_k^2 &= \mathcal{B}_{\text{sig}}^2 f_{\text{sig}}^2 \left(\frac{N_{\text{tot}}}{2m_\phi T} \right)^2 \left\{ n_{\text{bin}} [1 + 4\Delta t^2 m_\phi^2 - \cos(2m_\phi \Delta t)] \right. \\ &\quad \left. + 8m_\phi \Delta t \sin(m_\phi T) \cos(m_\phi T + 2\delta) + \cos(2m_\phi T + 4\delta) \sin(2m_\phi T) \tan(m_\phi \Delta t) \right\}. \end{aligned} \quad (\text{S11})$$

Using these expressions it is possible to calculate the χ^2 statistic for any choice of binning (for any value n_{bin}). Given Δt , T , N_{tot} , and α , we obtain a 90% confidence sensitivity estimate on \mathcal{B}_{sig} by requiring the branching ratio to be non-negative and utilizing the one-sided upper bound obtained by solving $\chi^2[\mathcal{B}_{\text{sig}}] = Z_{90}$, where $Z_{90} = 2.706$ is the solution to $\text{erf}(\sqrt{Z_{90}}/2) \equiv 0.9$ – for more details see Sec. 2c.

The behavior of numerical results in Figs. 2 and 3 can be understood by considering various limiting cases:

1. *Single bin.* First, let us consider a single time bin analysis, so that one does not resolve the oscillating signal. In this case, the χ^2 statistic in Eq. (S5) evaluates to

$$\chi_1^2 = \frac{\mathcal{B}_{\text{sig}}^2 f_{\text{sig}}^2 N_{\text{tot}}}{\mathcal{B}_{\text{bg}} f_{\text{bg}} (1 + \alpha^2 \mathcal{B}_{\text{bg}} f_{\text{bg}} N_{\text{tot}})} \left(1 + \frac{\sin(2m_\phi T + 2\delta) - \sin 2\delta}{2m_\phi T} \right)^2. \quad (\text{S12})$$

It is useful to compare χ_1^2 with the χ^2 for a signal constant in time,

$$\chi_{\text{const}}^2[\mathcal{B}] = \frac{n_{\text{bin}} S_{\text{bin}}^2}{\sigma_{\text{stat}}^2 + n_{\text{bin}} \sigma_{\text{sys}}^2} = \frac{(\mathcal{B} f_{\text{sig}} N_{\text{tot}})^2}{N_{\text{tot}} \mathcal{B}_{\text{bg}} f_{\text{bg}} + \alpha^2 (N_{\text{tot}} \mathcal{B}_{\text{bg}} f_{\text{bg}})^2} \quad (\text{S13})$$

where \mathcal{B} is the time-averaged $\ell_i \rightarrow \ell_j \phi$ branching ratio. The first equality follows from Eq. (S8) for a constant signal in each bin, $S_i = S_{\text{bin}}$, while the second equality uses that $S_{\text{bin}} = \mathcal{B} f_{\text{sig}} N_{\text{tot}} / n_{\text{bin}}$. In the limit of fast oscillations, i.e., for the case where the duration of the experiment is much longer than the oscillation period, $m_\phi T \gg 1$, one has $\mathcal{B}_{\text{sig}} = \langle 2\mathcal{B}_{\text{sig}} \cos^2(m_\phi t + \delta) \rangle$, giving for χ_1^2 in Eq. (S12)

$$\chi_1^2 \rightarrow \chi_{\text{const}}^2[\mathcal{B}_{\text{sig}}]. \quad (\text{S14})$$

That is, averaging χ_1^2 over time gives the value of χ^2 for a time-independent signal. In the limit of slow oscillations, $m_\phi T \ll 1$, Eq. (S12) becomes

$$\chi_1^2 \rightarrow \chi_{\text{const}}^2[\mathcal{B}_{\text{sig}} \cos^2(\delta)] + \mathcal{O}(m_\phi T). \quad (\text{S15})$$

The χ^2 test statistic is then sensitive to the phase δ of the classical field ϕ_c , resulting in a χ^2 that may be larger or smaller than the time-averaged signal with amplitude \mathcal{B}_{sig} . For $\delta = \pi/2$ the signal (and thus the χ^2) vanishes at leading order in $m_\phi T$; the first non-zero contribution to the signal is of order $(m_\phi T)^4$, resulting in a highly suppressed, but non-zero χ^2 .

2. *Coarse binning.* If the signal oscillates in the duration of the experiment ($m_\phi T \gg 1$), but the oscillation time is shorter than the bin size ($m_\phi \Delta t \gg 1$) the sensitivity to oscillations is decreased. In this limit the result for χ^2 is the same as the single bin result, Eq. (S14), because the binning is too coarse

$$\chi_{\text{cb}}^2 = \chi_{\text{const}}^2[\mathcal{B}_{\text{sig}}]. \quad (\text{S16})$$

3. *Fine binning.* If the binning is sufficiently small to resolve the oscillations ($m_\phi \Delta t \ll 1$) and the experiment runs long enough ($m_\phi T \gg 1$), then the χ^2 becomes

$$\chi_{\text{fb}}^2 = \frac{3}{2} \left(1 + \frac{\alpha^2 N_{\text{tot}} \mathcal{B}_{\text{bg}} f_{\text{bg}}}{3} \right) \chi_{\text{const}}^2[\mathcal{B}_{\text{sig}}] = \frac{3}{2} \left(1 + \frac{n_{\text{bin}} \sigma_{\text{sys}}^2}{3\sigma_{\text{stat}}^2} \right) \chi_{\text{const}}^2[\mathcal{B}_{\text{sig}}]. \quad (\text{S17})$$

When the systematic uncertainties can be ignored ($\alpha^2 N_{\text{tot}} f_{\text{bg}} \ll 1$) this fine binning performs slightly better than the course binning, $\chi_{\text{fb}}^2 = 3\chi_{\text{cb}}^2/2$. When systematic uncertainties dominate, however, fine binning does substantially better, resulting in a χ^2 that is not limited by the systematic uncertainty,

$$\chi_{\text{fb}}^2 = \frac{1}{2N_{\text{tot}} \mathcal{B}_{\text{bg}} f_{\text{bg}}} (\mathcal{B}_{\text{sig}} f_{\text{sig}} N_{\text{tot}})^2 = \frac{n_{\text{bin}} S_{\text{avg},1}^2}{2\sigma_{\text{stat}}^2}, \quad (\text{S18})$$

where $S_{\text{avg},1} \equiv \langle S_i \rangle = \mathcal{B}_{\text{sig}} f_{\text{sig}} N_{\text{tot}} / n_{\text{bin}}$. This result is intuitive: it is possible to measure a time-dependent signal even in the presence of large systematic uncertainties, as long as all the systematics are time independent.

b. Incoherent (“fast”) oscillations

For a given DM mass m_ϕ , the galactic halo’s typical velocity dispersion sets a characteristic coherence time, $\tau_{\text{coh}} \simeq (m_\phi v^2)^{-1}$, during which the classical DM background remains effectively in phase. When $m_\phi \gtrsim (v^2 T)^{-1}$, the total observation time T spans multiple coherence patches. To estimate the sensitivity to a DM signal in this regime, we account for decoherence by subdividing the observation period into $n_{\text{patch}} = \lceil T/\tau_{\text{coh}} \rceil = \lceil T m_\phi v^2 \rceil \simeq \lceil 10^{-6} m_\phi T \rceil$ equally spaced patches, where $\lceil \dots \rceil$ represents the ceiling function. Each patch $p \in \{1, 2, \dots, n_{\text{patch}}\}$ is assigned a

phase δ_p determined by minimizing the χ^2 statistic over the allowed phase variations. In the case $T/\tau_{\text{coh}} \in \mathbb{Z}$, the χ^2 is minimized when each patch maintains the same phase δ_{patch} , corresponding to the minimization with respect to δ over a single patch. For simplicity, in each patch we set $\delta_p = \delta_{\text{patch}}$ despite the possibility of a single partial patch not fully residing within the observation window T (assuming that the first patch starts at the beginning of the observation time). Including this additional minimization on the final partial patch does not meaningfully impact our derived sensitivities. To further simplify the analysis, we restrict the maximum size of each time bin to be the coherence time, $\Delta t \leq \tau_{\text{coh}}$, and limit the binning scheme to evenly divide the duration of a single patch, ensuring that no time bin traverses multiple patches. Under these approximations, the χ^2 statistic becomes

$$\begin{aligned} \chi^2 &= \frac{1}{N_{\text{bg},1}} \sum_{p=1}^{n_{\text{patch}}} \sum_{k=1}^{n_{\text{bin}}^p} S_k^2[\delta_p] - \frac{\alpha^2}{1 + \alpha^2 n_{\text{bin}} N_{\text{bg},1}} \left(\sum_{p=1}^{n_{\text{patch}}} \sum_{k=1}^{n_{\text{bin}}^p} S_k[\delta_p] \right)^2 \\ &\simeq n_{\text{patch}} \left[\frac{1}{N_{\text{bg},1}} \sum_{k=1}^{n_{\text{bin}}^{\text{patch}}} S_k^2[\delta_{\text{patch}}] - n_{\text{patch}} \frac{\alpha^2}{1 + \alpha^2 n_{\text{bin}} N_{\text{bg},1}} \left(\sum_{k=1}^{n_{\text{bin}}^{\text{patch}}} S_k[\delta_{\text{patch}}] \right)^2 \right] + \chi_{\text{partial}}^2, \end{aligned} \quad (\text{S19})$$

where the number of bins per patch is given by $n_{\text{bin}}^{\text{patch}} = \tau_{\text{coh}}/\Delta t = T/n_{\text{patch}}\Delta t = (m_\phi v^2 \Delta t)^{-1}$ and χ_{partial}^2 refers to the additional contribution to the χ^2 stemming from partial patches at the end of the observation time. Because of the fixed binning within each patch, a given Δt is not guaranteed to fit within a partial patch, introducing an error from integrating the signal over an additional amount of time dt_{extra} equivalent to

$$dt_{\text{extra}} = \left(\left\lceil \frac{\tau_{\text{coh}}(1 - n_{\text{patch}}) + T}{\Delta t} \right\rceil - \frac{\tau_{\text{coh}}(1 - n_{\text{patch}}) + T}{\Delta t} \right) \Delta t, \quad (\text{S20})$$

which vanishes as $\Delta t \rightarrow 0$ ($n_{\text{bin}}^{\text{patch}} \rightarrow \infty$). In the numerical examples presented in the main text, this error is accounted for explicitly in the computation of χ_{partial}^2 via subtraction of the extra contribution introduced by dt_{extra} . The χ^2 statistic and the derived sensitivity are computed analogously to the fully coherent case (using Eqs. (S10) and (S11)).

c. Time-independent signal

The χ^2 square statistic for a time-independent $\ell_i \rightarrow \ell_j \phi$ branching ratio $\mathcal{B}_{\text{const}}$ is given by $\chi_{\text{const}}^2[\mathcal{B}_{\text{const}}]$ in Eq. (S13). Again requiring $\mathcal{B}_{\text{const}}$ to be non-negative the one-sided upper bound at $X\%$ confidence level (CL) for $\mathcal{B}_{\text{const}}$, denoted as $\mathcal{B}_{\text{const}}^{X\% \text{CL}}$, is obtained by solving

$$\chi_{\text{const}}^2[\mathcal{B}_{\text{const}}] = Z_X \quad \text{with} \quad \text{erf}(\sqrt{Z_X}/2) \equiv (X/100). \quad (\text{S21})$$

For instance, $Z_{90} = 2.706$ and $Z_{95} = 3.841$. This yields

$$\mathcal{B}_{\text{const}}^{X\% \text{CL}} = \frac{1}{f_{\text{sig}}} \sqrt{Z_X \mathcal{B}_{\text{bg}} f_{\text{bg}} \left(\frac{1}{N_{\text{tot}}} + \mathcal{B}_{\text{bg}} f_{\text{bg}} \alpha^2 \right)} = \frac{1}{f_{\text{sig}} N_{\text{tot}}} \sqrt{Z_X n_{\text{bin}} (\sigma_{\text{stat}}^2 + n_{\text{bin}} \sigma_{\text{sys}}^2)}. \quad (\text{S22})$$

In the main text, Eq. (S22) was used to determine the systematic uncertainty parameter α for different experiments, given a quoted upper bound $\mathcal{B}_{\text{const}}^{X\% \text{CL}}$. For instance, for a systematic-dominated analysis ($\alpha^2 N_{\text{tot}} \mathcal{B}_{\text{bg}} f_{\text{bg}} \gg 1$), Eq. (S22) gives $\mathcal{B}_{\text{const}}^{X\% \text{CL}} \simeq \alpha \sqrt{Z_X} (\mathcal{B}_{\text{bg}} f_{\text{bg}} / f_{\text{sig}})$.

d. Discussion of time-dependent results

For time-dependent analysis we show in Fig. 2 in the main text, and in Fig. 3 in the supplemental material, the derived upper limits on the signal branching ratio of $\mu \rightarrow e\phi$, $\tau \rightarrow \mu\phi$ and $\tau \rightarrow \ell\phi$, respectively, as a function of the bin size in time (time resolution) Δt for different DM masses. For each mass and Δt , the phase δ is chosen by profiling the χ^2 over δ and selecting the value that minimizes the test statistic, ensuring the most conservative estimate. We see that for coarse time bins, in which the oscillatory nature of the signal cannot be resolved ($m_\phi \Delta t \gg 1$), the derived sensitivity is systematics limited. As Δt decreases and the time bins become finer, the oscillations start to be resolved, eventually becoming fully resolved around $\Delta t \sim m_\phi^{-1}$ (indicated by the vertical dotted lines). In this regime ($m_\phi \Delta t \ll 1$), the sensitivity is no longer systematics limited but instead becomes constrained by statistics.

The translated sensitivities on the scale f as a function of DM mass, using the most optimal time binning for each mass within the region of validity (between the gray regions denoted in Fig. 2), can be found in Fig. 1. That is, in the limit of fine-binning, given $T, N_{\text{tot}}, \mathcal{B}_{\text{bg}}, f_{\text{bg}}, f_{\text{sig}}$, and α , the 90% CL sensitivity estimates on \mathcal{B}_{sig} are obtained by demanding that $\chi^2 \leq Z_{90}$. Using Eqs. (9) and (S17), this requirement translates in the lower bound

$$\frac{f}{\sqrt{C_{ij}}} \geq \frac{8.9 \times 10^{-12} \text{ GeV}}{\sqrt{m_\phi}} \left(\frac{m_{\ell_i}^3}{\Gamma_{\ell_i}} \right)^{1/4} \left(\frac{N_{\text{tot}} f_{\text{sig}}^2 \left[3 + \mathcal{B}_{\text{bg}} f_{\text{bg}} \alpha^2 N_{\text{tot}} \right]}{\mathcal{B}_{\text{bg}} f_{\text{bg}} \left[1 + \mathcal{B}_{\text{bg}} f_{\text{bg}} \alpha^2 N_{\text{tot}} \right]} \right)^{1/8}, \quad (\text{S23})$$

where Γ_{ℓ_i} denotes the SM decay width of ℓ_i . Likewise in the limit of coarse-binning (or a single-bin analysis) the lower limit on f is given by

$$\frac{f}{\sqrt{C_{ij}}} \geq \frac{9.7 \times 10^{-12} \text{ GeV}}{\sqrt{m_\phi}} \left(\frac{m_{\ell_i}^3}{\Gamma_{\ell_i}} \right)^{1/4} \left(\frac{N_{\text{tot}} f_{\text{sig}}^2}{\mathcal{B}_{\text{bg}} f_{\text{bg}} (1 + \mathcal{B}_{\text{bg}} f_{\text{bg}} \alpha^2 N_{\text{tot}})} \right)^{1/8}. \quad (\text{S24})$$

Note that the derivation leading to Eq. (S17) has several implicit assumptions, all of which can fail:

- We assume that the data is collected continuously over the full observation time. More realistic experimental setups, where the observation window is broken into discrete chunks of continuous data-taking, can be taken into account with minimal and straightforward modifications to the analysis described above. Alternatively one could also use the Lomb-Scargle periodogram to search for the time-dependent signal [79].
- We assume that each time bin contains a sufficient number of events such that the statistic is χ^2 distributed. In our numerical analysis, we impose these boundaries as hard limits; for each experiment, we give estimates for improved sensitivity only for $m_\phi \in [1/T, n_{\text{bin}}^{\text{max}}/T]$, where $n_{\text{bin}}^{\text{max}} = N_{\text{tot}} f_{\text{bg}}/10$ is the largest number of bins such that each bin contains at least 10 events (background + signal). The regions outside the observational window $m_\phi \in [1/T, n_{\text{bin}}^{\text{max}}/T]$ are shaded in gray in Figs. (2) and (3).
- In Eq. (S17) we assume that the DM phase is fully coherent over the full observation time T . In a full experimental analysis, one must also properly account for the effect of phase coherence. As described in Sec. 2b, in our analysis, we account for DM decoherence approximately by considering $n_{\text{patch}} = T/\tau_{\text{coh}}$ equally spaced coherent patches where each patch maintains the same phase over its duration, chosen conservatively through a minimization of the test statistic over δ .

e. Experimental details

In this subsection we give further details about the treatment of experimental projections.

- **Mu3e $\mu \rightarrow e\phi$:** A defining feature of the $\mu \rightarrow e\phi$ signal are monoenergetic positrons at energy $E_e \simeq m_\mu/2$. This mono-energetic line lies at the endpoint of the SM decay $\mu \rightarrow e\nu\bar{\nu}$ ($\mathcal{B}_{\mu \rightarrow e\nu\bar{\nu}} = \mathcal{B}_{\text{bg}} \simeq 1$), given by the kinematic configuration of two neutrinos collinear that are back-to-back with the positron. The size of the background from the SM is determined by the detector's energy resolution. In our projections we take the positrons to be in the endpoint region, if their energy is within 3 MeV of the kinematic endpoint; this choice corresponds to the anticipated detector's intrinsic energy resolution [26–28], and is also comparable with the signal region used in the analysis in [52], where it was defined to be within $\simeq 4$ MeV of the endpoint, but also with a cut on the direction of positrons relative to muon spin. In this narrow window, the estimated background level is $N_{\text{bg}} \simeq 1.1 \times 10^{13}$, which is what we use in our projections. For comparison, widening the endpoint energy window to twice the resolution (i.e., 6 MeV) would increase the background yield to approximately 5.7×10^{13} events. Assuming, for simplicity, that the detection and reconstruction efficiencies are $\simeq 1$, we have $f_{\text{bg}} \simeq N_{\text{bg}}/N_{\text{tot}} = 3.3 \times 10^{-3}$. We also assume that the systematic uncertainties are dominated by the theory prediction on the SM background. This gives an expected 90%CL upper limit on $\mu \rightarrow e\phi$ branching ratio of $\mathcal{B}_{\text{const}}^{90\%} = 6 \times 10^{-7}$ (as determined in Ref. [52, Fig. 12]). From it we deduce the systematic uncertainty parameter α , assuming that approximately all of the signal events fall into this kinematic endpoint ($f_{\text{sig}} \simeq 1$) as well as systematics domination ($\alpha^2 N_{\text{tot}} \mathcal{B}_{\text{bg}} f_{\text{bg}} \gg 1$) in Eq. (S22), giving $\alpha \simeq (\mathcal{B}_{\text{const}}^{90\%} f_{\text{sig}})/(\sqrt{Z_{90}} \mathcal{B}_{\text{bg}} f_{\text{bg}}) = 1.1 \times 10^{-4}$.
- **Belle-II $\tau \rightarrow \ell\phi$:** During the 2019-2020 run, Belle-II recorded roughly $N_{\text{tot}} \simeq 1.2 \times 10^8$ taus [25] (we assume that these were collected continuously over 300 days). Of these, approximately $\mathcal{B}_{\tau \rightarrow e\nu\bar{\nu}} = 17.8\%$ (for $\ell = e$) and $\mathcal{B}_{\tau \rightarrow \mu\nu\bar{\nu}} = 17.4\%$ (for $\ell = \mu$) decay via the SM channel $\tau \rightarrow \ell\nu\bar{\nu}$ [80]. The Belle-II analysis also requires the

tag hemisphere to contain three charged particles, $\tau \rightarrow 3h\nu_\tau$, $h = \pi, K$, with a branching $\mathcal{B}_{\tau \rightarrow 3h\nu} = 15.2\%$ [80]. The irreducible SM background (available for the analysis) thus has a branching of

$$B_{\text{bg}}^{e[\mu]} \simeq 2.7 \times 10^{-2} \left(\frac{\mathcal{B}_{\tau \rightarrow \ell\nu\bar{\nu}}}{0.178[0.174]} \right) \left(\frac{\mathcal{B}_{\tau \rightarrow 3h\nu}}{0.152} \right). \quad (\text{S25})$$

In the tau pseudo-rest frame the distribution of charged lepton energy E_ℓ^* for these SM decays resembles the one expected from the exotic $\tau \rightarrow \ell\phi$ decays, since the poor reconstruction of the tau rest frame smears the mono-energetic signature. In Belle-II shape information was used to distinguish between background and signal. In our estimates we instead use a simplified strategy, and define signal regions as the energy windows $E_e^*/(m_\tau/2) \in [0.66, 1.48]$ and $E_\mu^*/(m_\tau/2) \in [0.71, 1.38]$ defined to retain $\epsilon_{\text{cut}}^{\text{sig}} \simeq 90\%$ of the $\tau \rightarrow \ell\phi$ signal events, N_{sig} , and straddle symmetrically the peak of the signal distribution. These windows simultaneously capture about $\epsilon_{\text{cut}}^{\text{bg},e} \simeq 59\%$ and $\epsilon_{\text{cut}}^{\text{bg},\mu} \simeq 56\%$ of the SM background events, N_{bg} , for electrons and muons, respectively. Moreover, the minimal reconstruction efficiency for the signal channel is estimated at $\epsilon_{\text{rec}}^{\text{sig},e} \simeq 13.4\%$ for electrons and $\epsilon_{\text{rec}}^{\text{sig},\mu} \simeq 17.4\%$ for muons [81, Table 4.4], while for the background $\epsilon_{\text{rec}}^{\text{bg},e} \simeq 12.7\%$ and $\epsilon_{\text{rec}}^{\text{bg},\mu} \simeq 16.2\%$ [25, 81]. Combining the kinematic cuts and the reconstruction efficiencies yields

$$f_{\text{bg}}^{e[\mu]} \simeq 7.5 \times 10^{-2} [9.1 \times 10^{-2}] \left(\frac{\epsilon_{\text{cut}}}{0.59[0.56]} \right) \left(\frac{\epsilon_{\text{rec}}}{0.127[0.162]} \right), \quad (\text{S26})$$

$$f_{\text{sig}}^{e[\mu]} \simeq 0.12 [0.16] \left(\frac{\epsilon_{\text{cut}}}{0.9} \right) \left(\frac{\epsilon_{\text{rec}}}{0.134[0.174]} \right). \quad (\text{S27})$$

These agree within 30% with the values one would obtain if the results in Fig. 1 in [25] were used instead. Using the relation $\alpha \simeq (\mathcal{B}_{\text{const}}^{90\%} f_{\text{sig}})/(\sqrt{Z_{90}} \mathcal{B}_{\text{bg}} f_{\text{bg}})$ in Eq. (S22) with the 90% confidence-level limits $\mathcal{B}_{\text{const}}^{90\%} \simeq 7.6 \times 10^{-4}$ for electrons and 4.7×10^{-4} for muons [25, Tab. III], we obtain systematic uncertainty parameters of $\alpha \simeq 2.7 \times 10^{-2}$ and $\alpha \simeq 1.9 \times 10^{-2}$ for the electron and muon channels, respectively. For the full Belle-II analysis utilizing the entire 50 ab^{-1} integrated luminosity dataset, we provide sensitivity projections using the same analysis outlined above (with an appropriately rescaled N_{tot}) assuming that the time integrated analysis will remain systematics dominated at the present value. While this is very likely to be too conservative, given that improvements in both the systematics and the observables used to distinguish between signal and background are likely [82], the approximation suffices for our purposes: the rough estimate of the reach for the time-dependent analysis.

- **FCC-ee $\tau \rightarrow \ell\phi$** : While running in Tera-Z mode the proposed FCC-ee experiment will produce approximately $N_{\text{tot}} = 2N_{\tau\bar{\tau}} \simeq 2 \times 1.7 \times 10^{11}$ taus over $T = 740$ days of running [30]. While the changes in the boost of the taus, coverage of the detector, and energy resolution will doubtless lead to changes in signal and background separation, to date there have not been detailed studies of the expected reach for the $\tau \rightarrow \ell\phi$ channel at FCC. Here, for simplicity, we assume a similar analysis and background contamination to that of Belle-II, and take the reconstruction efficiency to be $\epsilon_{\text{rec}}^{\text{sig,bg}} \simeq 90\%$. Ignoring small differences between e and μ this gives

$$f_{\text{bg}} \simeq 0.53 \left(\frac{\epsilon_{\text{cut}}}{0.59} \right) \left(\frac{\epsilon_{\text{rec}}}{0.9} \right), \quad (\text{S28})$$

$$f_{\text{sig}} \simeq 0.81 \left(\frac{\epsilon_{\text{cut}}}{0.9} \right) \left(\frac{\epsilon_{\text{rec}}}{0.9} \right). \quad (\text{S29})$$

As a surrogate for the expected bound on $\tau \rightarrow \ell\phi$ we use the expected systematics dominated (absolute) precision on the leptonic branching fraction of $\sigma(\mathcal{B}_\ell) = 3 \times 10^{-5}$. It is hoped that, even if the final precision is systematically limited, it will not be far from this value [83]. Using $\alpha \simeq \sigma(\mathcal{B}_\ell) f_{\text{sig}}/(\mathcal{B}_{\text{bg}} f_{\text{bg}})$ with \mathcal{B}_{bg} in Eq. (S25), we find $\alpha \simeq 1.7 \times 10^{-3}$.